Supplementary Information

Constructing multi-interface engineering of NiS/Ni_3S_2/Fe_3O_4 nanoarchitectures for use as high-efficiency electrocatalysts toward oxygen evolution reaction

Chengcheng Li, Anyang Bao, Cuizhen Yang, Guoqiang Liu, Xiang Chen, Mengyue Li, Yuwen Cheng, Dongming Liu*

School of Materials Science and Engineering, Anhui University of Technology, Maanshan, Anhui 243002, China

Contents

in the region of 0.2-0.3 V vs. RHE.

Fig. S16. Specific activity of NP-(Fe,Ni)-S, NP-Ni-S, NP-(Fe,Ni) and NP-Ni normalized by their corresponding ECSA.

Fig. S17. LSV curves before and after 3000 CV cycles of NP-(Fe,Ni)-S.

Fig. S18. XRD patterns of NP-(Fe,Ni)-S before and after OER test in 1.0 M KOH.

Fig. S19. High-resolution XPS spectra of S 2p for NP-(Fe,Ni)-S before and after OER test.

Fig. S20. XRD patterns of NP-Ni-S before and after OER test in 1.0 M KOH.

Fig. S21. SEM image of NP-Ni-S after OER test in 1.0 M KOH.

Fig. S22. High-resolution XPS spectra of (a) O 1s and (b) S 2p of NP-Ni-S before and after OER test in 1.0 M KOH.

Fig. S23. Raman spectrum of NP-Ni-S after OER test in 1.0 M KOH.

Table S1. Specific surface area and pore size of NP-(Fe,Ni) and NP-(Fe,Ni)-S.

Table S2. Comparison of OER activity of NP-(Fe,Ni)-S in 1.0 M KOH with other advanced reported non-noble metal electrocatalysts.

1. Experimental sections

1.1 Synthesis of NP-Ni electrocatalyst

The $NiAl_3$ alloy precursor was prepared by magnetically levitated induction melting of Ni and Al strips with molar ratio of 1:3 under argon atmosphere. Then, the $NiAl_3$ ingots were ball-milled for 12 h under argon atmosphere. The nano-porous Ni (NP-Ni) was synthesized by a previous reported work via alkali-etching of the $NiAl_3$ powders under 10 wt% NaOH solution at 25 °C.

1.2 Synthesis of NP-Ni-S electrocatalyst

The NP-Ni-S was synthesized through a traditional hydrothermal method by employing NP-Ni (0.1 g) powder, thiourea (3 mmol) and deionized water (60 mL) to prepare homogeneous solution. The solution was placed into a 100 ml Teflon-lined stainless-steel autoclave before kept at 150 °C for 6 h in an oven. After cool-down to room temperature, the NP-Ni-S was collected and dried at 60 °C for 12 h after filtering and washing with deionized water for several times.

2. Figures

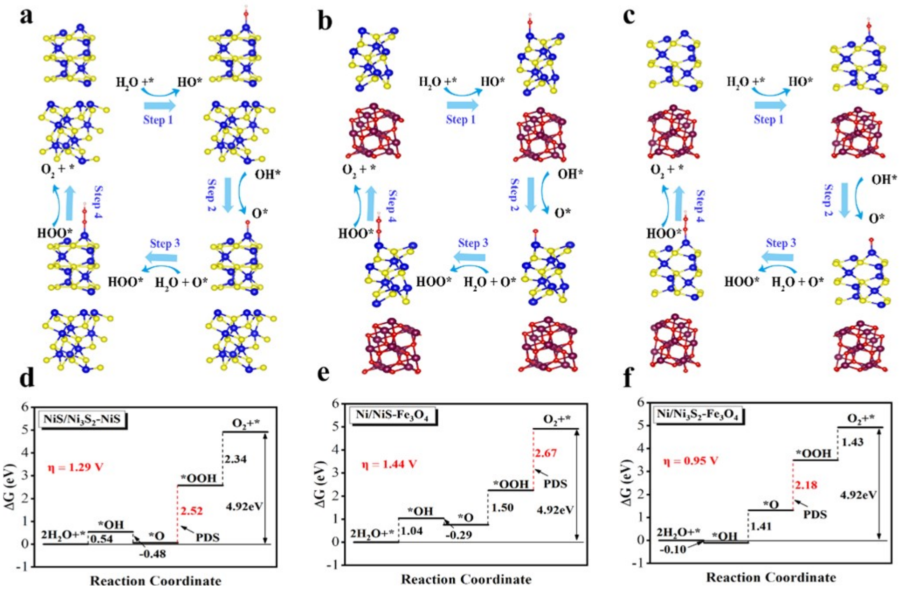

Fig. S1. Four-electron mechanism of OER on (a) Ni_3S_2-NiS, (b) Fe_3O_4-NiS, and (c) Ni_3S_2-Fe_3O_4 model. (d–f) Calculated free-energy diagram of OER intermediates at zero potential (U=0).

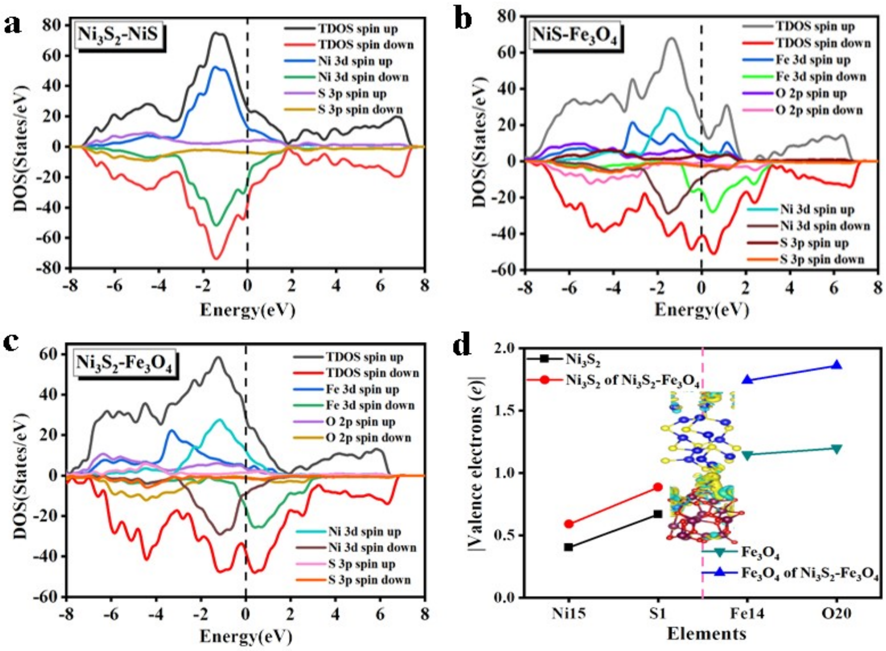

Fig. S2. Density of states of (a) Ni_3S_2-NiS, (b) NiS-Fe_3O_4 and (c) Ni_3S_2-Fe_3O_4. (d) The absolute valence electrons for Ni_3S_2, Fe_3O_4, as well as Ni_3S_2 and Fe_3O_4 of Ni_3S_2-Fe_3O_4. The inset represents the charge difference density of Ni_3S_2-Fe_3O_4.

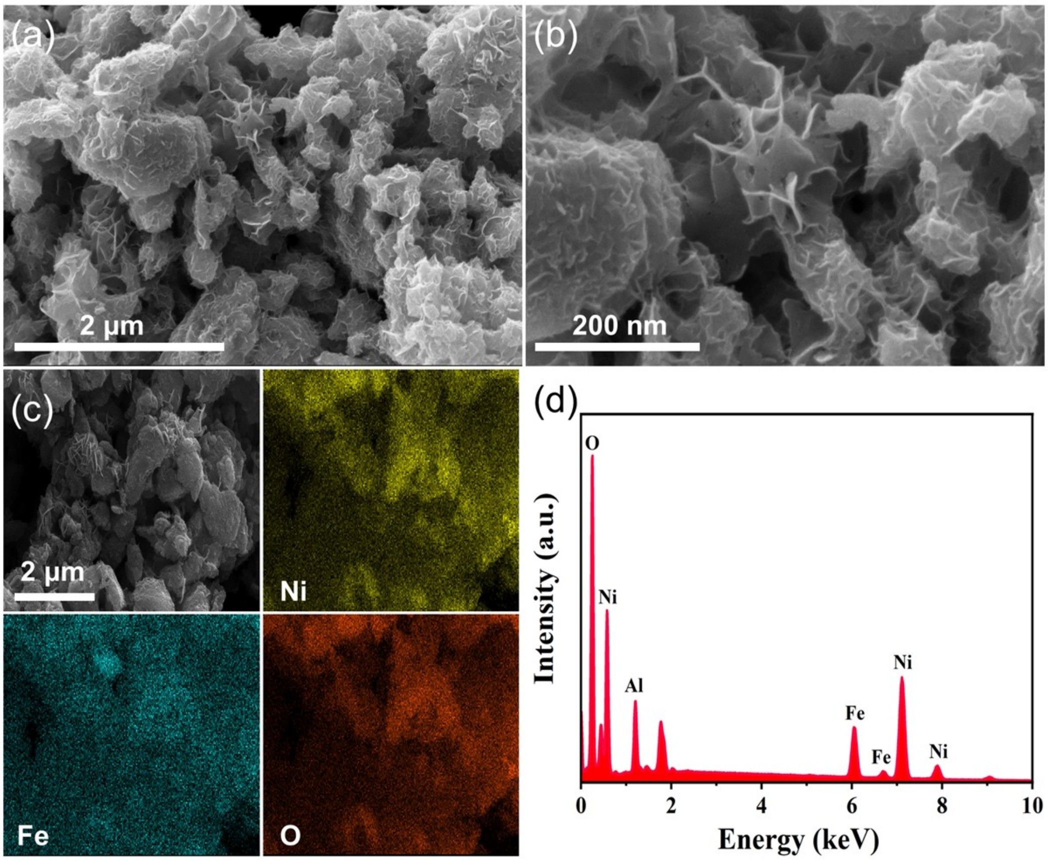

Fig. S3. (a-b) SEM images of NP-(Fe,Ni) at different magnifications. (c) EDX mapping images of Fe, Ni and O for NP-(Fe,Ni). (d) EDX spectrum of NP-(Fe,Ni).

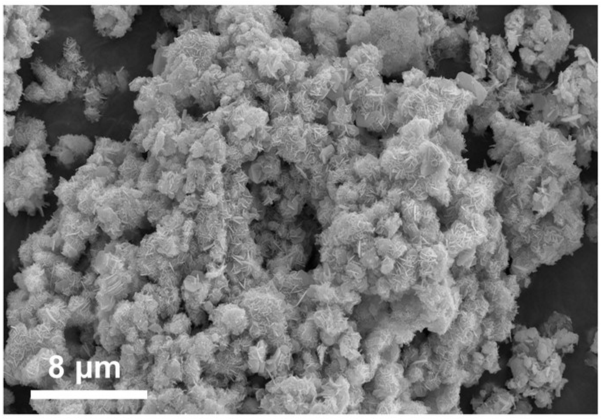

Fig. S4. SEM image of NP-(Fe,Ni)-S.

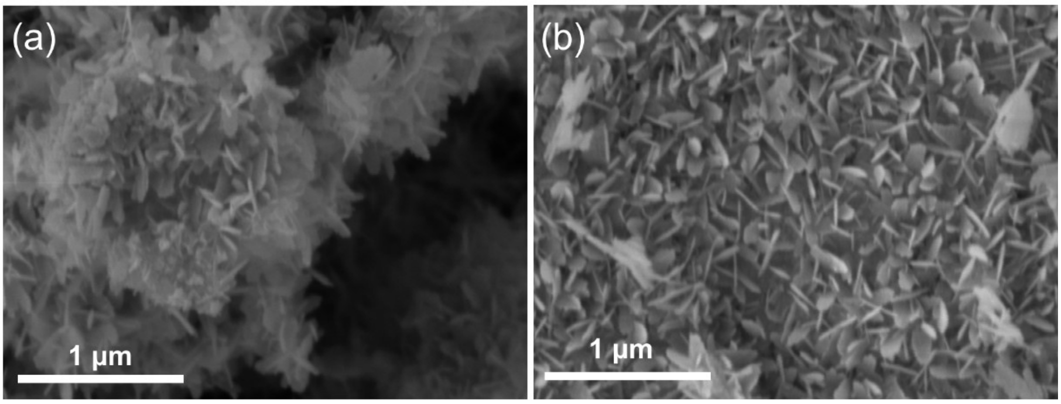

Fig. S5. SEM images of NP-Ni-S.

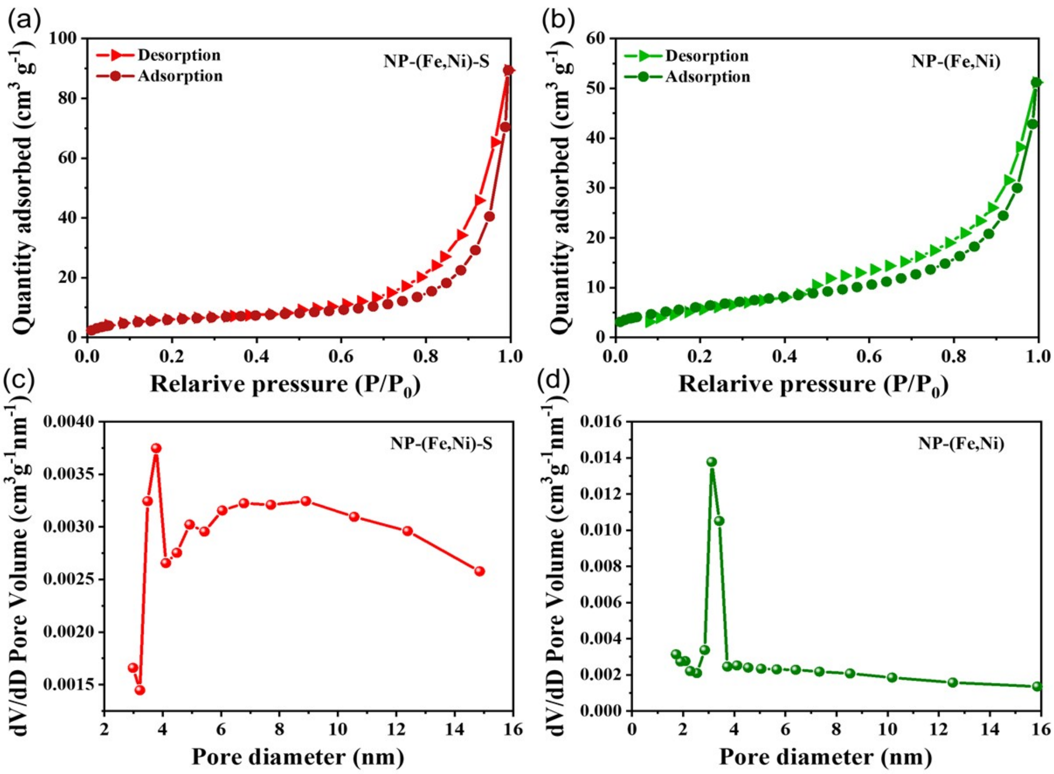

Fig. S6. (a-b) N_2 adsorption/desorption isotherms and (c-d) pore size distribution plots of NP-(Fe,Ni) and NP-(Fe,Ni)-S.

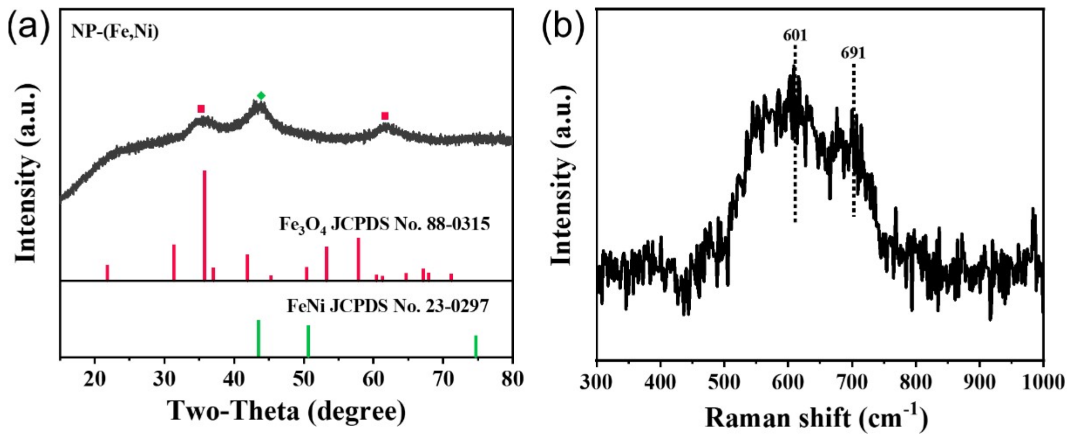

Fig. S7. (a) XRD pattern of NP-(Fe,Ni). (b) Raman spectrum of NP-(Fe,Ni).

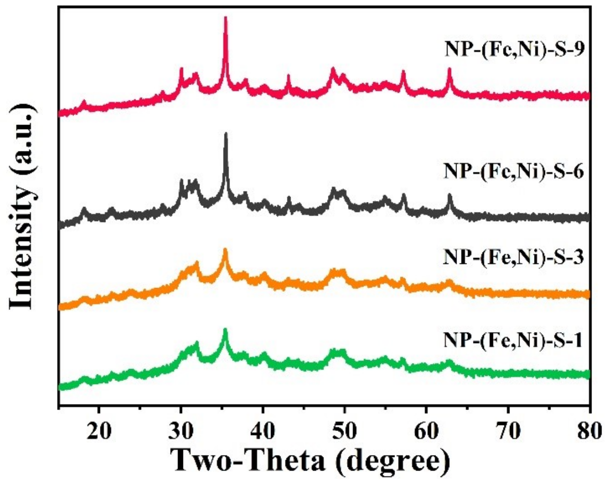

Fig. S8. XRD patterns of NP-(Fe,Ni)-S-*x* with sulfurization times of 1, 3, 6, and 9 h.

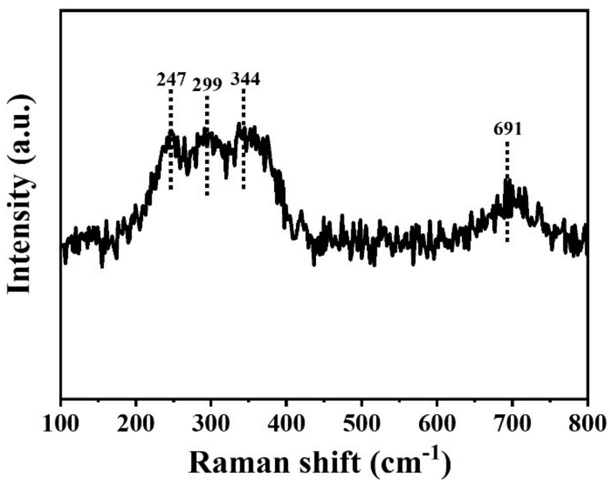

Fig. S9. Raman spectrum of NP-(Fe,Ni)-S.

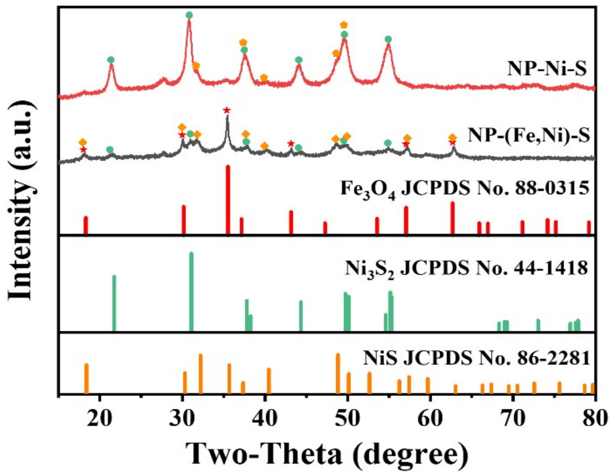

Fig. S10. (a) XRD patterns of NP-Ni-S and NP-(Fe,Ni)-S.

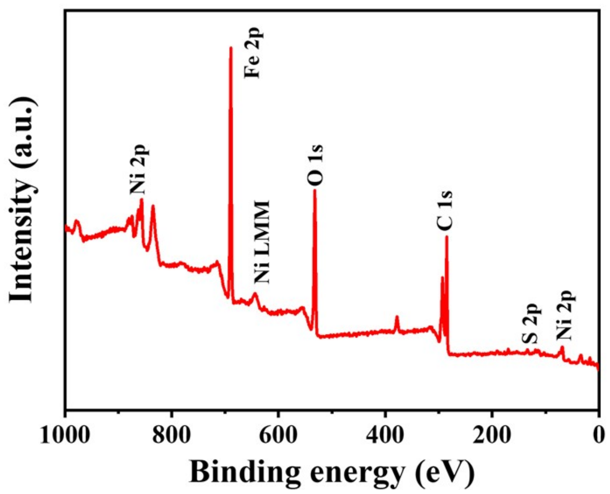

Fig. S11. The XPS survey spectrum of NP-(Fe,Ni)-S.

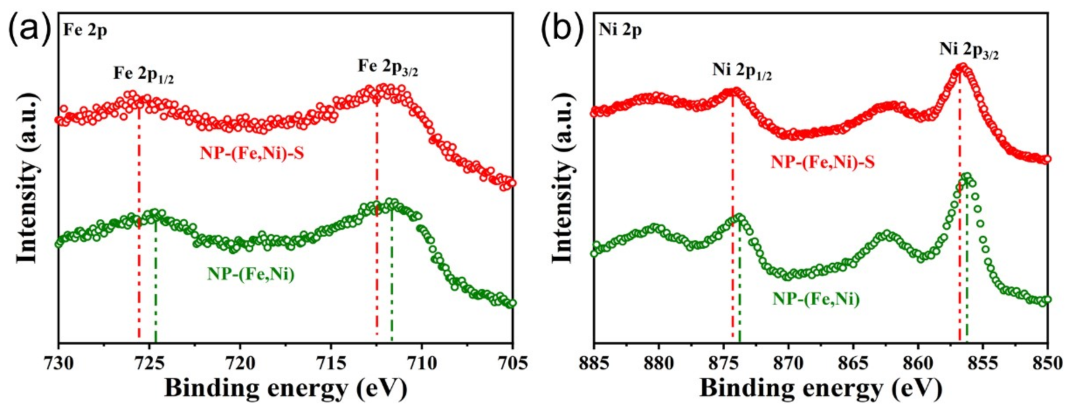

Fig. S12. High-resolution XPS spectra of (a) Fe 2p and (b) Ni 2p for NP-(Fe,Ni) and NP-(Fe,Ni)-S.

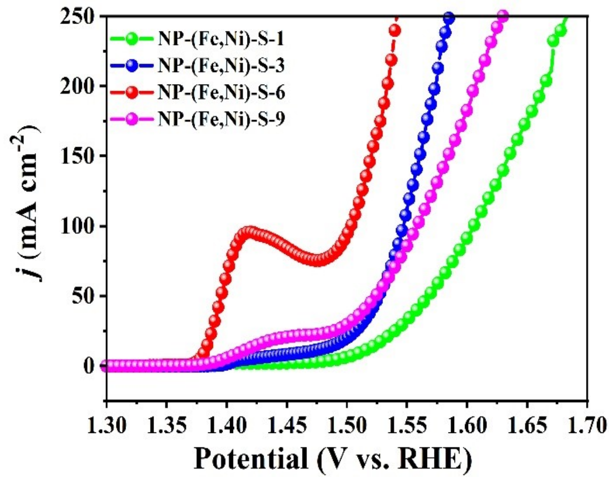

Fig. S13. OER LSV curves of pristine NP-(Fe,Ni)-S-1, NP-(Fe,Ni)-S-3, NP-(Fe,Ni)-S-6, NP-(Fe,Ni)-S-9 in 1.0 M KOH electrolyte at a scan rate of 5 mV s^{-1}.

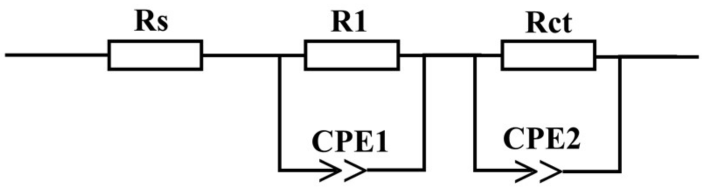

Fig. S14. The equivalent circuit used to fit the Nyquist plots.

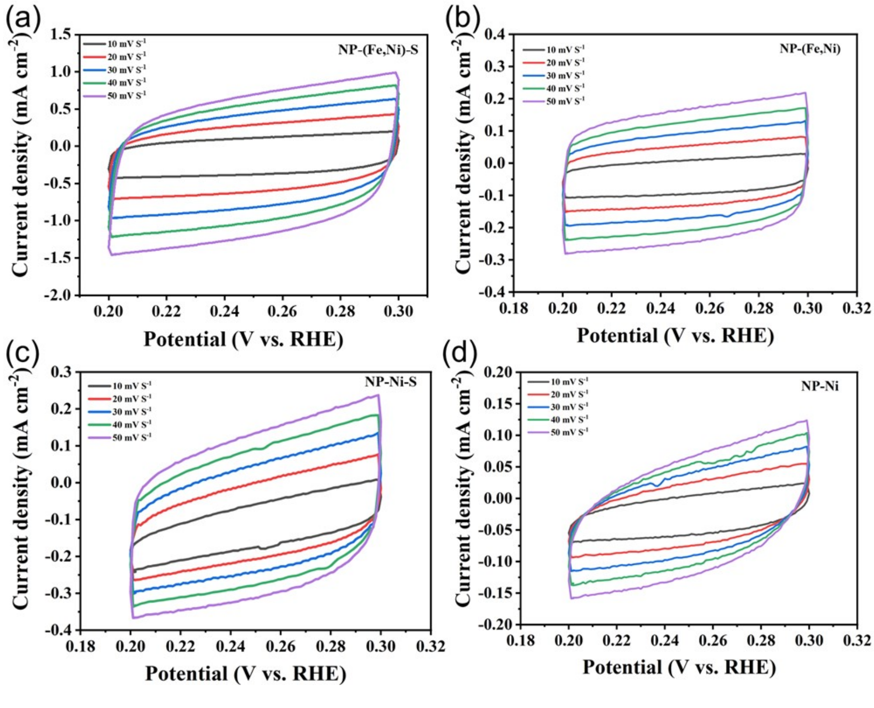

Fig. S15. CV curves of NP-(Fe,Ni)-S, NP-(Fe,Ni), NP-Ni-S and NP-Ni at different scan rates in the region of 0.2-0.3 V vs. RHE.

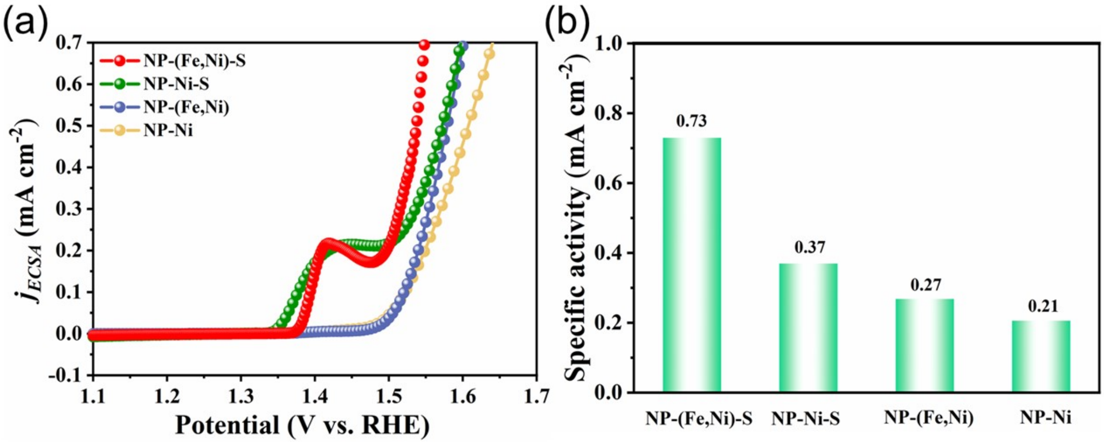

Fig. S16. Specific activity of NP-(Fe,Ni)-S, NP-Ni-S, NP-(Fe,Ni) and NP-Ni normalized by their corresponding ECSA.

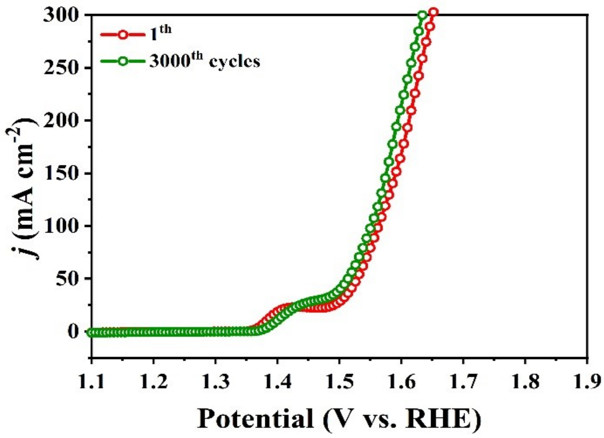

Fig. S17. LSV curves before and after 3000 CV cycles of NP-(Fe,Ni)-S.

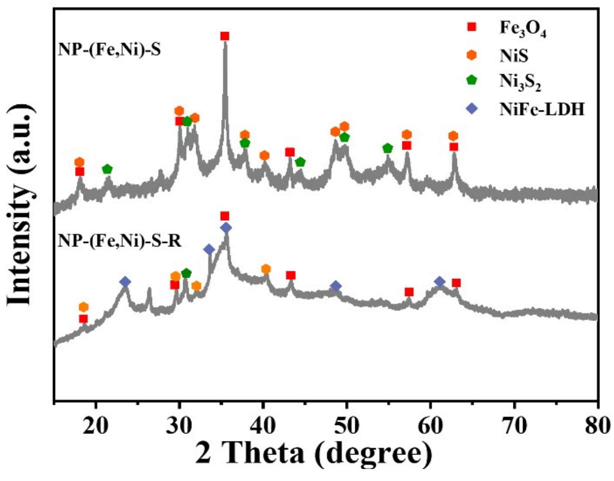

Fig. S18. XRD patterns of NP-(Fe,Ni)-S before and after OER test in 1.0 M KOH.

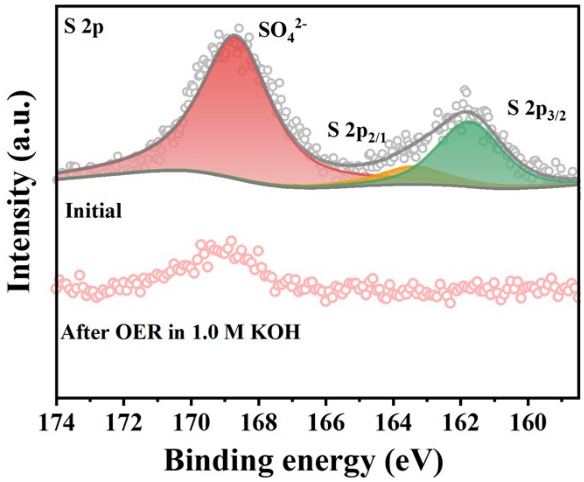

Fig. S19. High-resolution XPS spectra of S 2p for NP-(Fe,Ni)-S before and after OER test.

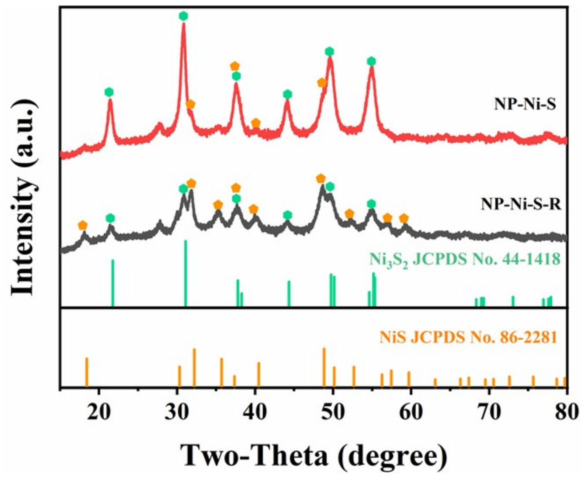

Fig. S20. XRD patterns of NP-Ni-S before and after OER test in 1.0 M KOH.

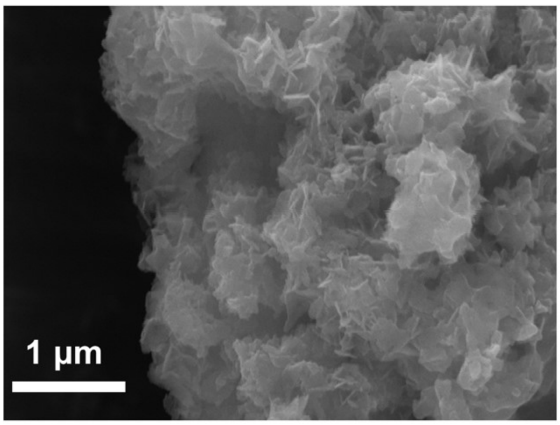

Fig. S21. SEM image of NP-Ni-S after OER test in 1.0 M KOH.

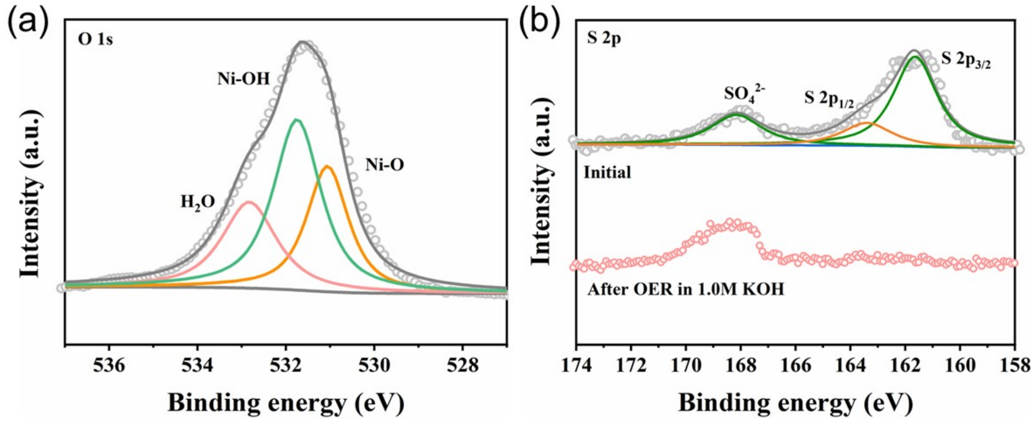

Fig. S22. High-resolution XPS spectra of (a) O 1s and (b) S 2p of NP-Ni-S before and after OER test in 1.0 M KOH.

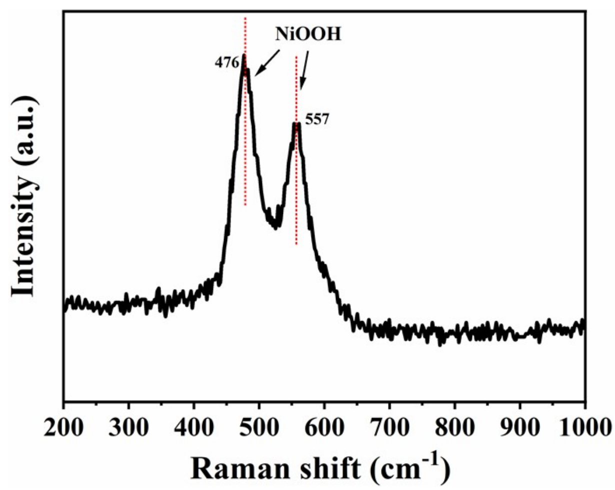

Fig. S23. Raman spectrum of NP-Ni-S after OER test in 1.0 M KOH.

Table S1. Specific surface area and pore size of NP-(Fe,Ni) and NP-(Fe,Ni)-S.

Samples	Specific surface area ($m^2\ g^{-1}$)	Pore size (nm)
NP-(Fe,Ni)	23.4	5.3
NP-(Fe,Ni)-S	21.3	8.3

Table S2. Comparison of OER activity of NP-(Fe,Ni)-S in 1.0 M KOH with other advanced reported non-noble metal electrocatalysts.

Catalysts	Overpotential (mV) at 100 mA cm^{-2}	Ref.
NP-(Fe,Ni)-S	274	This work
Ni-Fe/$NiMoN_x$	292	1
NiMoN/NF-450	370	2
Ni/$NiFeMoO_x$/NF	289	3
Ni_2P-VP_2/NF	398	4
MoO_x/Ni_3S_2/NF	310	5
Pd/$NiFeO_x$	296	6
NiS/NiS_2	416	7
ZnP@Ni_2P-$NiSe_2$	326	8
Fe-Ni_2P@Cu_xS	390	9
$NiCo_2S_4$	399	10
NiFe-LDH	302	11
Ni_3FeN/r-Go	320	12

References

1 Y. Qiu, M. Sun, J. Cheng, J. Sun, D. Sun, L. Zhang, Bifunctional Ni-Fe/NiMoN$_x$ nanosheets on Ni foam for high-efficiency and durable overall water splitting, *Catal. Commun.,* 2022, **164**, 106426.

2 Y. Wang, Y. Sun, F. Yan, C. Zhu, P. Gao, X. Zhang, Y. Chen, Self-supported NiMo-based nanowire arrays as bifunctional electrocatalysts for full water splitting, *J. Mater. Chem. A.,* 2018, **6,** 8479-8487.

3 Y. Li, G. Zhang, W. Lu, F. Cao, Amorphous Ni-Fe-Mo suboxides coupled with Ni network as porous nanoplate array on nickel foam: A highly efficient and durable bifunctional electrode for overall water splitting, *Adv. Sci.,* 2020, **7,** 1902034.

4 H. Yan, Y. Xie, A. Wu, Z. Cai, L. Wang, C. Tian, X. Zhang, H. Fu, Anion-modulated HER and OER activities of 3D Ni-V-based interstitial compound heterojunctions for high-efficiency and stable overall water splitting, *Adv. Mater.,* 2019, **31,** 1901174.

5 Y. Wu, G. Li, Y. Liu, L. Yang, X. Lian, T. Asefa, X. Zou, Overall water splitting catalyzed efficiently by an ultrathin nanosheet-built, hollow Ni_3S_2-based electrocatalyst, *Adv. Funct. Mater.,* 2016, **26,** 4839-4847.

6 W. Zhang, X. Jiang, Z. Dong, J. Wang, N. Zhang, J. Liu, G. Xu, L. Wang. Porous Pd/NiFeO$_x$ nanosheets enhance the pH-universal overall water splitting, *Adv. Funct. Mater.,* 2021, **31,** 2107181.

7 Q. Li, D. Wang, C. Han, X. Ma, Qi. Lu, Z. Xing, X. Yang, Construction of amorphous interface in an interwoven NiS/NiS_2 structure for enhanced overall water splitting, *J.*

Mater. Chem. A., 2018, **6,** 8233-8237.

8 K. Chang, D. T. Tran, J. Wang, S. Prabhakaran, D.H. Kim, N.H. Kim, J.H. Lee, Atomic heterointerface engineering of Ni_2P-$NiSe_2$ nanosheets coupled ZnP-based arrays for high efficiency solar-assisted water splitting, *Adv. Funct. Mater.,* 2022, 2113224.

9 D.T. Tran, H.T. Le, V.H. Hoa, N.H. Kim, J.H. Lee, Dual-coupling ultrasmall iron-Ni_2P into P-doped porous carbon sheets assembled Cu_xS nanobrush arrays for overall water splitting, *Nano Energy,* 2021, **84,** 105861.

10 G. Janani, S. Yuvaraj, S. Surendran, Y. Chae, Y. Sim, S. Song, W. Park, M. Kim, U. Sim, Enhanced bifunctional electrocatalytic activity of Ni-Co bimetallic chalcogenides for efficient water-splitting application, *J. Alloys Compd.,* 2020, **846,** 156389.

11 X. Wang, Y. Tuo, Y. Zhou, D. Wang, S. Wang, J. Zhang, Ta-doping triggered electronic structural engineering and strain effect in NiFe LDH for enhanced water oxidation, *Chem. Eng. J.,* 2021, **403,** 126297.

12 Y. Gu, S. Chen, J. Ren, Y. Jia, C. Chen, S. Komarneni, D. Yang, X. Yao, Electronic structure tuning in Ni_3FeN/r-GO aerogel toward bifunctional electrocatalyst for overall water splitting, *ACS Nano,* 2018, **12**, 245-253.